The fate of microplastics in estuary: A quantitative simulation approach

Zilin Shen[a,b], Hua Wang [a, b,*], Dongfang Liang[c], Yuting Yan[a,b], Yichuan Zeng[a,b]

[a] Key Laboratory of Integrated Regulation and Resource Development on Shallow Lake of Ministry of Education, College of Environment, Hohai University, Nanjing 210098, China;

[b] College of Environment, Hohai University, Nanjing 210098, China;

c Department of Engineering, University of Cambridge, Cambridge CB2 1PZ, UK;

*. Corresponding author's e-mail: wanghua543543@163.com.

Abstract: Microplastics pollution is an emerging environmental concern. However, there are almost no MPs numerical simulation studies in the Yangtze Estuary which is considered as the largest plastic export in the world and quantitative simulation is not carried out in the existing models. Therefore, completing quantitative simulation and exploring different patterns of MPs transport are the main objectives of this study. In addition, the concentration distribution and risk of MPs are also analyzed. Mass-Number method is proposed to quantitatively simulate microplastics concentration in Feb. and May with errors of less than 18%. Compared with sediment flocculation and settling transport, independent floating transport is more susceptible to surface currents resulting in increased beaching and more inhomogeneous concentration distribution. Meanwhile, under the influence of current, local topography and salt wedge, the MPs perform linear motion and clockwise spiral motion inside and outside the estuary and rapidly form a "hot spot" on the southeastern part of Chongming Island and 57% to 90% of MPs are beached or settled inside the estuary, especially on the north shore. Therefore, MPs risk in some sensitive targets should be concerned according to risk assessment results. Our results break the space-time limit and explore the fate of MPs in the Yangtze Estuary and provide new idea and concern of MPs numerical simulation.

Keywords: Microplastics; Quantitative simulation; Transport patterns; Pollution risk

1 Introduction

As early as the 1970s, humans have discovered the existence of microplastics (MPs) (< 5mm) in the ocean (Carpente.Ej et al. 1972). The Fifth United Nations Environment Assembly held in 2022 have established the first global treaty to tackle plastic pollution. Plastic debris is now ubiquitous throughout both marine and freshwater environment (Ling et al. 2017). MPs take advantage of huge specific surface area and hydrophobic functional groups absorbing dissolved organic matter and they are easily ingested by marine organisms such as zooplankton, invertebrates and fish and then pass and accumulate along food chain through predatory activities (Derraik 2002, Zhang et al. 2020, Farrell and Nelson 2013). Subsequently, contaminated microplastics not only have toxic effects on organisms but also pose immeasurable potential risks to ecosystem and human (Castelvetro et al. 2020, Derraik 2002).

Numerical simulation studies of MPs have been carried out in only a few estuaries, coasts and bays in the world. A dynamic study of MPs along the coast of South Africa found that different destinations for high-density and low-density MPs (Collins and Hermes 2019). The study in the Arabian/Northwest Persian Gulf has showed that wind condition has a significant impact on the transport and distribution of MPs (Alosairi et al. 2020). The study in Jervis Bay has found that relative to turbulent dispersion and washing-off, MPs fates are more sensitive to MPs dynamical properties, in particular plastic density and biofilm properties (Iwasaki et al. 2017). The simulation of MPs in Delaware Bay has indicated that the buoyant particles created “hot spots” within hours (Cohen et al. 2019). In China, a Short-Term MPs simulation has been carried out in Lai Zhou Bay (Ding et al. 2019). Previous study focused on changes in particles trajectories under the influence of weather and MPs dynamics. But the chemical composition of MPs is not considered. It is worth noting that the chemical composition of MPs is diverse and significantly affects the transport pattern of MPs (He et al. 2021). Lots of research have been shown that the type of MPs can determine the pattern of settlement, individual or aggregation with suspended sediment due to different aggregation barrier

(Andersen et al. 2021, Kaiser et al. 2017, Li et al. 2019). What's more, previous simulation studies only focused on the trajectories. Thus, a quantitative simulation of MPs for different chemical compositions is presented in this study. Around 51% of Global plastic is produced in Asia (Mai et al. 2020). The Yangtze River, the largest river in Asia, is considered to be the largest plastic export river to the ocean in all existing modeling studies (Schmidt et al. 2018). However, there is no study on numerical simulation of MPs in the Yangtze Estuary. Therefore, the aims of the present study are as follows: (1) Based on previous field sampling, a quantitative simulation of MPs concentration (MPC) is implemented. (2) Different simulations for MPs with different chemical compositions is performed. (3) The characteristics of MPC distribution are analyzed. (4) Risk analysis of MPs in sensitive areas is performed.

2 Methods and Materials

2.1 Study Area

The Yangtze River located in the subtropical monsoon climate is the third longest and fifth largest river in terms of discharge volume (~900km^3yr^{-1}) in the world (Wang et al. 2020). The Yangtze River receives a large number of materials from a drainage area of $1.8\times10^6km^2$, encompassing 1/6 of China (Feng et al. 2014).

Due to the prosperous economy and dense population, the annual use of agricultural plastic film in the Yangtze River Basin is about 610000 tons, which is significantly higher than that in other basins (according to China Environment Statistics Yearbook stats.gov.cn) and due to the COVID-19 pandemic, disposable surgical masks have also become a non-negligible plastic pollution, especially in the densely populated Yangtze River basin (Shen et al. 2021). Therefore, the Yangtze River is considered to be the largest plastic-export river to the ocean (Schmidt et al. 2018). What's more, a generally increasing trend of MPs abundance from upstream to downstream is identified, which is attributed to the geographical and anthropogenic factors (Feng et al. 2014, Yuan et al. 2022, He et al. 2021) (Fig.1 b). Through the investigate in downstream, the abundance of MPs in lakes and estuary is significantly higher than that in rivers (Li et al. 2019, Zhang et al. 2020) (Fig.1 b). The abundance of MPs in estuary and ocean is 4137±2461.5 and 0.167±0.138

n/m^3 respectively, which indicates that the estuary is filter of MPs (Zhao et al. 2014).

There are three reservoirs and three animal refuges in the estuary and two animal refuges with different conservation objectives overlap each other in the east of Chongming Island (Fig.1 c). These animal refuges are established to protect endangered species such as Chinese sturgeon, paddlefish, and migratory birds that occur most frequently in spring (Zeng et al. 2021). The freshwater resource and biodiversity of the Yangtze Estuary make the research on MPs in this region of great value.

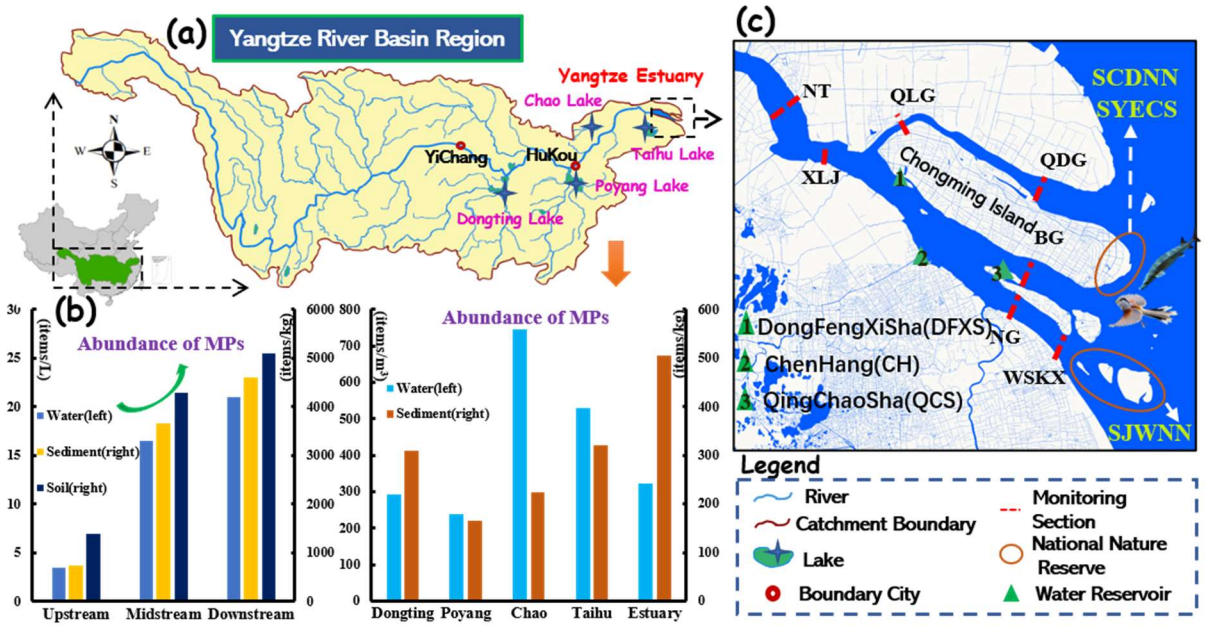

Figure 1 Study Area, (a) Yangtze River Basin Map; (b) Distribution characteristics of microplastics in the Yangtze River Basin (Li et al. 2019, Yuan et al. 2022); (c) Yangtze Estuary Map.

2.2 Data Collection

The model terrain and bathymetric data is provided by Taile Maps (http://www.arctiler.com/). Model ocean boundary data comes from National Marine Data Center, National Science & Technology Resource Sharing Service Platform of China (http://mds.nmdis.org.cn/) and tide data is provided by Hydrology and Water Resources Survey Bureau of Yangtze Estuary. Since the scope of Chongming District is almost the same as that of the Yangtze Estuary, meteorological data for simulation, which were measured in Chongming District, involving daily average wind speed and direction, precipitation, evaporation and temperature, comes from National Centers for Environmental

Information (https://www.ncei.noaa.gov/maps/daily/) and Wheat A databases (http://www.wheata.cn/). Monitoring cross sections are shown in Fig.1 c and their details are provided by previous research (Wang et al. 2019, 2020, Zeng et al.). The salinity is measured by ion chromatography and conforms to the standard SL86-1994. The water temperature is measured by a thermometer and conforms to national standard GB/T 13195-1991, and the suspended solid concentration (SSC) is measured by the gravimetric method and conforms to the national standard GB/T11901-1989.

2.3 Simulated MPs Determination

Based on our bibliographic search, there are only nine studies relative to the distribution and abundance of MPs in water of the Yangtze Estuary in "ScienceDirect" database. The sampling tools, especially the sieve pore size, have significant impact on the MPC (Dubaish and Liebezeit 2013). The average abundance of MPs detected by 32μm and 70μm steel screens in wet season is 4137.3±2461.5 n/m^3 and 231±182 n/m^3 respectively, which are significantly difference (Xu et al. 2018, Zhao et al. 2014). Water season and rainfall also affect MPC (Williams and Simmons 1999). The field detection of abundance of MPs of the Yangtze Estuary in Feb., May and Jul. has shown that the MPC in the dry season is significantly higher than that in wet season (Zhao et al. 2019).

The shape, material, size and color of MPs are also the focus of research (Li et al. 2021). Almost all studies have shown that the MPs in Yangtze Estuary are mainly fibrous (77.8%-91.6%), followed by fragments (15.1%) (Li et al. 2020, Wang et al. 2019, Xu et al. 2018, Zhao et al. 2019, Zhao et al. 2014). What's more, the MPs detected in the Yangtze Estuary are mainly polyethylene (PE, 82.4%) and polypropylene (PP, 9.1%). The high-density MPs are mainly polyvinyl chloride (PVC, 6.5%) (Xu et al. 2018). MPs with particle size smaller than 1mm account for 68.2%-82.3%, and MPs with particle size of 0.5-1mm account for 67% (Fig.2 a). However, the lack of a uniform standard for the color of MPs has led to large difference between research results (Fig.2 b).

Based on the above, we generalize the MPs in the Yangtze Estuary into fibrous particles with length and diameter of

0.8 mm and 100 μm, respectively (Chubarenko et al. 2016). Meanwhile, since PE MP, PP MP and PVC MP account for 84.5%, 9.1% and 6.5% in the Yangtze Estuary, we choose these three types of MPs for simulation.

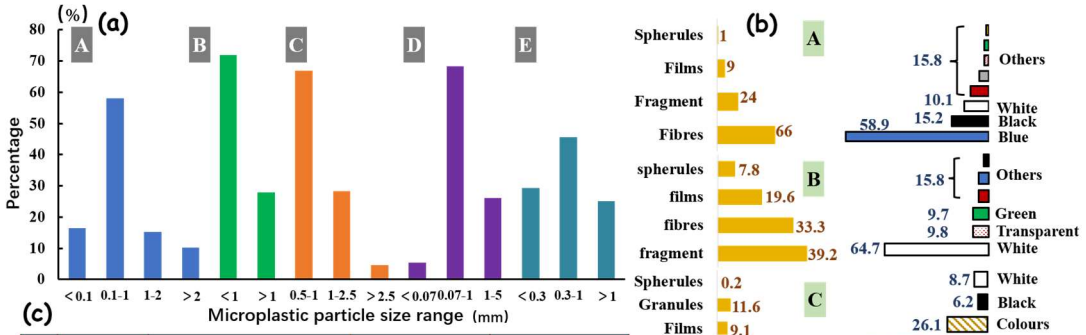

(c)

	Mesh Size	Time	MPs abundance	Reference
A	60μm	Apr. to Sept. in 2017	900 n/m^3	(Luo et al. 2019)
B	32μm	Jun. in 2019	67.5±94.4 n/m^3	(Li et al. 2020)
C	20μm	Jul. in 2013	500-10200 n/m^3	(Zhao et al. 2014)
D	300μm	Aug. in 2017	231±182 n/m^3	(Xu et al. 2018)
E	70μm	Feb., May and Jul. in 2017	157.2±75.8 n/m^3	(Zhao et al. 2019)

Figure 2 Microplastic characteristics in the Yangtze Estuary, (a) Size characteristic; (b) Shape and Color characteristics; (c) References.

2.4 Numerical Model Experiment

2.4.1 Simulation Scheme

A variety of precious species gather at the Yangtze Estuary from Mar. to Jun. every year to lay eggs, raise young, forage and inhabit. Therefore, this period is called biological sensitive period (Fig.3 a). Especially, April 15th to May 15th each year is the common residence period of endangered species Chinese Sturgeon and migration birds. Therefore, we select this period to simulate the concentration distribution of three types of MPs and analyze the risk in the sensitive areas. Moreover, in order to ensure the accuracy of simulation, we simulate the MPC in Feb. and May 2017 and compare the results with the measured data in previous literature (Zhao et al. 2019).

We consider the wind speed, precipitation and evaporation as the meteorological condition (Fig.3 b c). The simulation year is 2017.

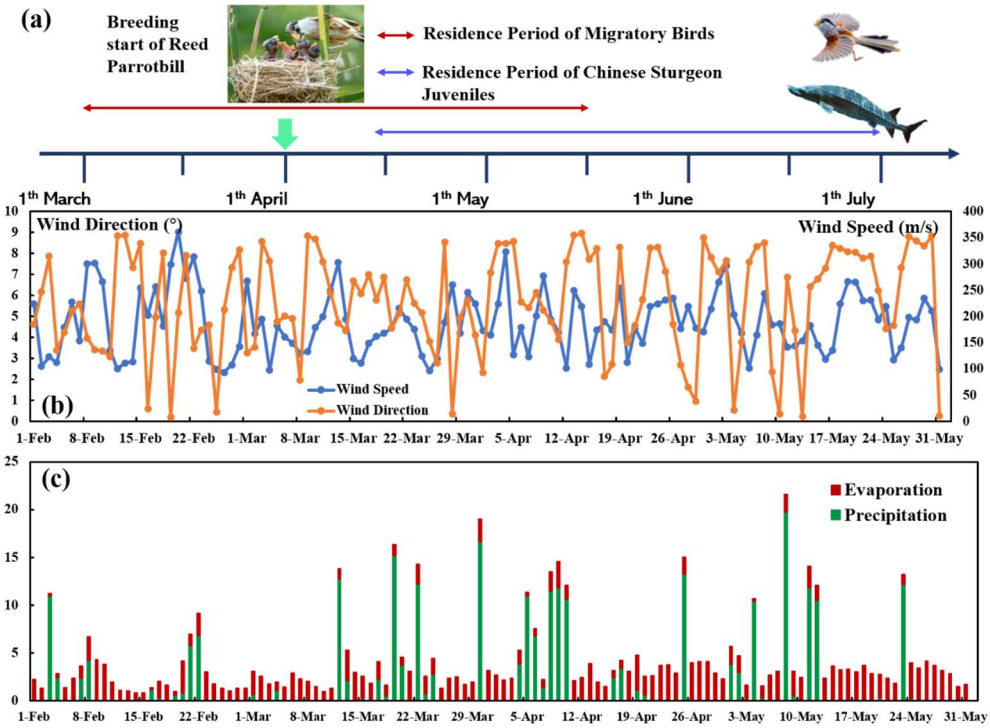

Figure 3 Simulation scheme, (a) Biological sensitive period; (b) Wind condition; (c) Evaporation and Precipitation conditions.

2.4.2 Model Selection

Aggregation behavior, including homogeneous and heterogeneous aggregation, is an important feature of plastic transport processes (Besseling et al. 2017). Compared with nano-plastics, the homogeneous aggregation of MPs is difficult (Wang et al. 2021). More than that, the probability of heterogeneous aggregation of MPs is much higher than that of homogeneous aggregation (Long et al. 2015, Singh et al. 2019).

MPs biofouling and suspended sediment flocculation are two main ways of heterogeneous aggregation (Long et al. 2015, Long et al. 2017). The chemical composition of MPs significantly affects heterogeneous aggregation behavior. Biofilms are observed on the surface of PP MPs within several days (Lagarde et al. 2016). In high-turbidity estuarine and coastal environment, PVC MPs readily flocculate with fine-grained natural suspended sediment (Andersen et al. 2021, Huffer et al. 2017, Li et al. 2019, Pohl et al. 2020). However, as the result of aggregation barrier, fibrous PE MPs not only hardly flocculate with sediment but also are difficult to be bio-fouled (Lagarde et al. 2016, Li et al. 2019). Fibrous and spherical PE MPs retain in the euphotic zone for 6~8 months and 10~15 years, respectively

(Chubarenko et al. 2016, Kaiser et al. 2017).

Based on above statement and density of three types of MPs (Fig.4), PE MP is considered as drifting particle with zero sinking velocity without heterogeneous aggregation. PP MP is considered as drifting particle whose settling velocity varies with biofilm growth. PVC MP is considered as particle transported by flocculation with fine-grained suspended sediment (< 16μm). PE MPs and PP MPs are independent settling particles and PVC MPs are flocculated particles. Although this is not absolute, the main possible transport patterns of these three types of MPs are used to explore the difference of different transport patterns.

There are lots of uncertainties of resuspended and aging processes of MPs (Zhang 2017, Kowalski et al. 2016). Therefore, the numerical simulation of MPs rarely considers these processes. In this study, there periods (one month each) are selected for MPs simulation. Since the aging of MPs is a very slow process, it may have little effect on the results in this study (Kowalski et al. 2016, Welden and Cowie 2017). Meanwhile, although this simplification may bring some inaccuracies, Atwood believes that a simplified approach is preferable to setting an arbitrary factor (Atwood et al. 2019). Therefore, these processes are not considered in the model. But these processes need to be explored according to experiment in the future to improve simulation accuracy.

2.4.3 Behavior Parameterization

The Lagrangian tracking model is implemented to simulate the transport of three types of MPs. For independent settling particles, MPs behavior mainly depends on three characteristics: density; shape; and size (Chubarenko et al. 2016, Khatmullina and Isachenko 2017, Kooi et al. 2017). Several studies suggest that biofouling can be visible after several days/weeks (Kooi et al. 2017). Biofouling of MPs is a complex process affected by various factors such as algal concentration, light and salinity (Kaiser et al. 2017) and is rarely considered in other simulation studies. However, in order to gain insight into the importance of this process, the empirical value in Jervis Bay is used for the biofouling rate, 5×10^{-4} mm/day (Jalon-Rojas et al. 2019). For the settling velocity of fibrous MPs, both models

proposed by Khatmullina et al. and Waldschlager et al. overestimate the settling velocity, with average errors of 74.1% and 34.3%, respectively and the model proposed by Dioguardi et al. underestimate the settling velocity, with an average error of 64.5%. Compared with these models, the model proposed by Zhang et al. can better estimate the settling velocity of the fibrous with an average error of 18.8% (Dioguardi et al. 2018, Khatmullina and Isachenko 2017, Waldschlager and Schuttrumpf 2019, Zhang and Choi 2022). Meanwhile, the formula is developed for drag coefficient and settling velocity of non-spherical particles (Zhu and Zeng 2016).

Thus, fibrous MPs settling velocity:

$$C_D = \frac{58.58 ASF^{0.1936}}{R_e^{0.8273}} \quad (1.)$$

$$ASF = \frac{D_L D_S}{D_I} \quad (2.)$$

$$R_e = \frac{u_t d_{eq}}{\vartheta} \quad (3.)$$

$$C_D = \frac{4}{3} \frac{D_{eqv}^{\ 3}}{d_{eq}^2 u_t^2} \frac{\rho_m - \rho_w}{\rho_w} g \quad (4.)$$

$$d_{eq} = \sqrt{4 D_L D_I / \pi} \quad (5.)$$

$$V = \frac{D_{eqv}^3 \pi}{6} \quad (6.)$$

where C_D is drag coefficient, ASF is Aschenbrenner shape factor, R_e is Reynolds number, ϑ is kinematic viscosity of the fluid, u_t is settling velocity, V is the volume of a microplastic, ρ_m is the particle density, ρ_w is the fluid density, g is the gravitational acceleration, d_{eq} and D_{eqv} are equivalent diameter of maximum cross-sectional area and volume of microplastic, respectively, D_L, D_I and D_S are the longest, intermediate and shortest lengths of a microplastic, respectively, Herein, for fibrous microplastic, D_I=D_S=2*r and D_L=l (Fig.4).

Biofouling process causes changes in the size and density of MPs. Thus, density and size of bio-fouled fibrous MPs (Chubarenko et al. 2016):

$$\rho_m = \rho_0 \frac{r^2}{(r+d)^2} + \rho_f \left[1 - \frac{r^2}{(r+d)^2}\right] \quad (7.)$$

$$D_I = D_S = 2 \times (r + d) \quad (8.)$$

where ρ_0 is the density of PP MP, 0.946 g/cm^3, ρ_f is the density of biofilm, 1.2 g/cm^3 (Fisher et al. 1983, Macleod et al. 2016), d is the thickness of biofilm, r is the radius of fibrous (Fig.4).

According to above formulas, we simulate the transport process of biofouling PP MPs. The initial conditions of MPs need to be considered when biofouling MPs are simulated. That means not all MPs are clean when released. Since biofilm growth is measured in days, we classified MPs into 31 contaminated states.

For sediment flocculated particles, the presence of MPs has no significant effect on the dispersion of suspended sediment (Andersen et al. 2021). Therefore, the transport of PVC MPs is simulated by simulating the diffusion of fine-grained sediment (< 16μm). Due to the lack of research on the distribution law of MPs in the solid and liquid phases, the model simplifies the positive correlation between the amount of PVC MPs and concentration of fine-grained sediment. Form fine-grained sediment flux and MPs flux in XLJ, it is obtained that each kilogram of fine-grained sediment (< 16μm) contains about 0.023g MPs. The suspended sediment is divided into four fractions (< 16μm, 16~32μm, 32~64μm, > 64μm) according to the content of sediment of different fractions (Gao et al. 2018).

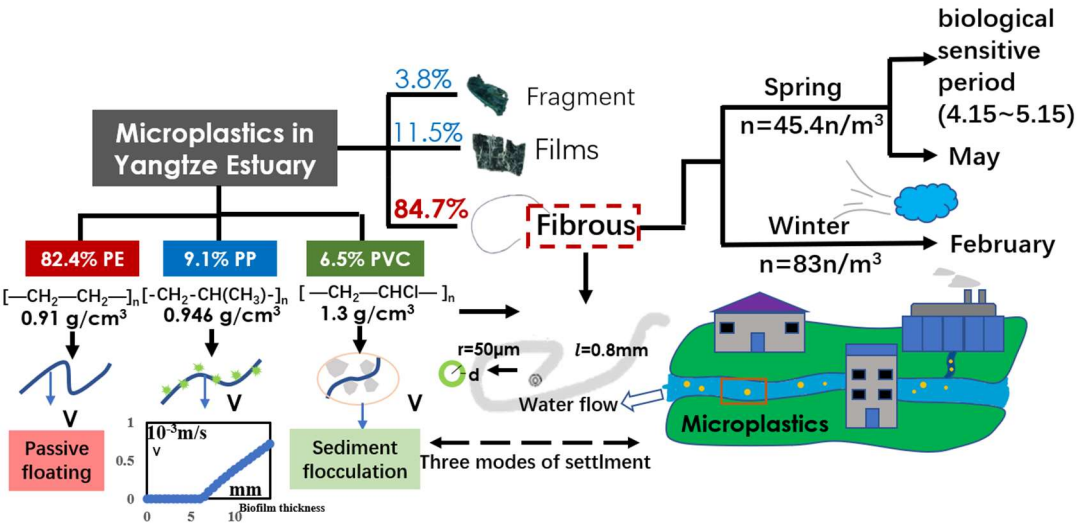

Figure 4 Model Selection and Behavior Parameterization.

2.4.4 Governing Equations

Water current simulation

The water current is simulated by hydrological model of MIKE 21. The hydrodynamic control module equations are

195 in DHI (DHI, 2011a).

196 **Sediment transport simulation**

197 Since resuspended process is not considered, the settling process is focused. Suspended sediment transportation is
198 simulated in fraction groups. With low concentration of suspended sediment, due to the low probability of collision
199 between cohesive particles, it is a possibility to give a rough estimate of the settling velocity of a single free particle
200 through Stokes law. With increasing concentration, flocculation and hindered settling need to be considered.

201 The settling velocity formulation of single particle is as followed:

202 $$\boldsymbol{w_0 = \frac{(\rho_s - \rho) g d^2}{18 \rho v}} \quad (9.)$$

203 Where w_0 is settling velocity of single particle, m^3/s, ρ_s is sediment dry density, 2650 kg/m^3, ρ is water density,
204 kg/m^3, g is gravity acceleration, $9.82 m/s^2$, d is grain size, m, v is dynamic viscosity, m^2/s.

205 The settling velocity formulations of particles with flocculation and hindered processes are as followed:

206 $$\boldsymbol{w_s = w_0 \times factor_{floc}} \quad (10.)$$

207 $$\boldsymbol{C_{total} \leq C_{floc} \quad factor_{floc} = 1} \quad (11.)$$

208 $$\boldsymbol{C_{floc} < C_{total} < C_{hindered} \quad factor_{floc} = 1 + \propto \left(\frac{C_{total}}{C_{floc}} - 1 \right)} \quad (12.)$$

209 $$\boldsymbol{C_{total} \geq C_{hindered} \quad factor_{floc} = 1 + \propto \left(\frac{C_{hindered}}{C_{floc}} - 1 \right)} \quad (13.)$$

210 Where w_s is the particle settling velocity, m^3/s, C_{total} is total sediment concentration, kg/m^3, c_{floc} is flocculation
211 critical sediment concentration, $0.01 kg/m^3$, $c_{hindered}$ is hindering critical sediment concentration, 7.8 kg/m^3, $\propto$ is
212 gradient coefficient, for calibration (DHI, 2011c).

213 **Particle tracking simulation**

214 The random walk particle tracking model is used to simulate the transport of suspended substances discharged in
215 estuaries. The model can be described as advection and reformulate as diffusion is also included.

216 $$\boldsymbol{X^{t+\Delta t} = X^t + U \Delta t + R(t) \sqrt{2 K_h \Delta t}} \quad (14.)$$

Where X^t and $X^{t+\Delta t}$ are the passive particle position vector time of t and $t+\Delta t$; U is the velocity vector of model flow field; Δt is the time step of the random walk; $R(t)$ is a uniformly distributed random number in the interval, which is given by Fortran 90 random number generator; K_h is the eddy diffusion coefficient of the horizontal random walk, which is derived from the hydrodynamic model (DHI, 2011d).

2.5 Mathematical Analysis Method

Quantitative evaluation of MPC

The average MPs fluxes of surface water in the Yangtze Estuary in spring and winter in 2017 are 45.4n/m^{3}and 83n/m^3, respectively (Zhao et al. 2019). Based on measured flow, the release of MPs per second in May and Feb. 2017 is 31114n and 24983n, respectively. The huge release quantity of MPs is the difficulty of numerical quantitative simulation. According to experiments, the average mass of MPs is 3.3×10^{-5}g (Zhao et al. 2019). Assuming that the mass of a single MP remains unchanged, a quantitative simulation method for MPs based on the Mass-Number (M-N) relationship is proposed. At present, almost only the surface water and sediment of the Yangtze Estuary have been carried out field sampling and measurement. Therefore, we implement numerical simulation research on MPs for surface water.

The relationship between MPC and mass concentration of MPs:

$$\boldsymbol{MPC} = \frac{\boldsymbol{M} \times \boldsymbol{10^{-6}}}{\boldsymbol{w} \times \boldsymbol{m}} \quad (15.)$$

Where, $\boldsymbol{M}$ is the mass concentration of MPs, which is obtained by averaging the values of each grid in one region, $\boldsymbol{w}$ is the surface water coefficient referring to 30 cm depth, which is 0.022 in winter and spring (Zhao et al. 2019), $\boldsymbol{m}$ is the average mass of MPs, 3.3×10^{-5} g.

In addition, two methods, HI and PLI, are used to assess the risk of MPs and the specific calculation methods are in the Appendix (Yin et al. 2021, Xu et al. 2018).

3 Results and Discussion

3.1 Model Performance

The model area is 4.08×10^4 km^2, including four inflow boundaries (Yangtze River, Qiantang River, Huangpu River, Zhoushan River) and three outflow boundaries (South of Yellow Sea, East China Sea and Pacific Ocean). In order to ensure the accuracy of model, we give a total of 6494 nodes and 10588 triangular elements for the modeling area and set 60 seconds as the calculation time step of the model. The CFL (Courant Friedrich Levy) number is less than 0.8 to meet the requirement of model stability. The hydrodynamic and sediment parameters are set according to Wang et al. and Zeng et al (Wang et al. 2020, Zeng et al. 2021). The Kolmogorov-Smirnov (K-S) test, Relative Coefficient (R^2) and Relative Error (E) are adopted to judge the accuracy of model according to the flow and SSC data measured in XLJ (Fig.5 b c). This process ensures the accuracy of the simulation environment.

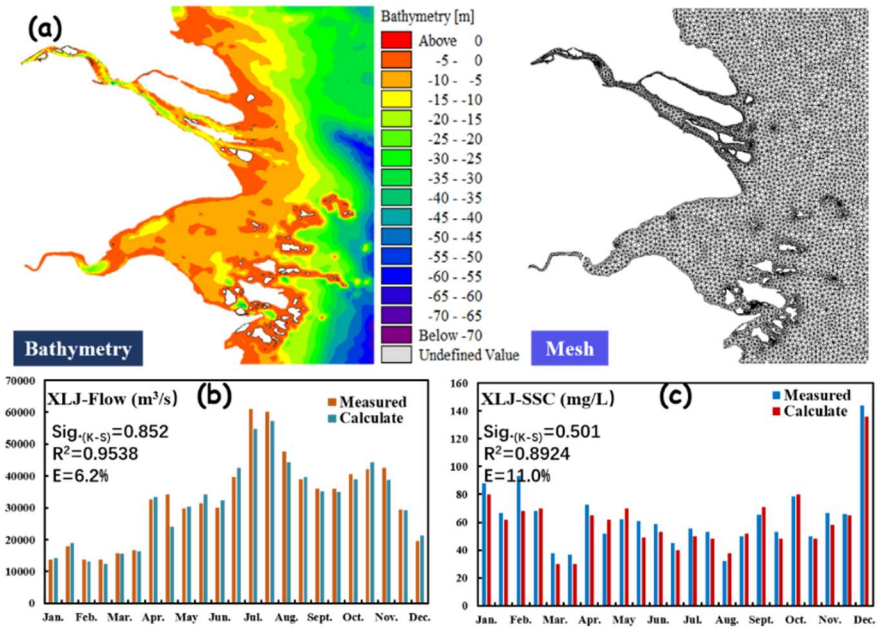

Figure 5 Model Performance, (a) Bathymetry and Mesh of the Yangtze Estuary; (b) Flow validation; (c) Suspended solid concentration validation.

Since almost all MPs in the surface water of the Yangtze Estuary are PE MPs (Zhao et al. 2014), the simulated concentrations of PE MPs in dry season (Feb.) and wet season (May) in 2017 are used to compare with measured data from Zhao et al. in same periods (Zhao et al. 2019) to complete quantitative simulation using M-N method and verify simulation accuracy.

The Yangtze Estuary and adjacent sea area are divided into eight parts (Fig.6 a). The total MPs concentration (TMPC)

256 in A, B and C are 545 n/m^3, 254 n/m^3 and 131 n/m^3 in Feb., respectively and the TMPC in A, B and C are 484 n/m^3,
257 462 n/m^3 and 177 n/m^3 in May, respectively. These are much higher than measured values (Fig.6 a). The reason is
258 that the beaching of MPs is not considered. This phenomenon is also emphasized in the study of the Sea of Japan
259 (Iwasaki et al. 2017) and the simulated study in marine around South Africa have indicated that half of the sewage
260 outlets have more than 90% of MPs beached (Collins and Hermes 2019). Xiong et al. also have found that a
261 considerable number of MPs from the large river catchment do not reach the sea (Xiong et al. 2019). When beaching
262 of MPs is considered, the suspended MPs concentration (SMPC) in A, B and C are 111 n/m^3, 107 n/m^3 and 52 n/m^3
263 in Feb., respectively and the SMPC in A, B and C are 64 n/m^3, 52 n/m^3 and 36 n/m^3 in May, respectively. The average
264 errors between the measured and simulated values in Feb. and May are 17.6% and 16.9% in the estuary, respectively.
265 The beaching rate of MPs in the estuary are around 73.6% and 83.8% in Feb. and May, respectively (Fig.6 b). In the
266 adjacent sea area, almost no MPs beaching occurs. The simulated MPC in E, F, G and H are 41 n/m^3, 123 n/m^3, 188
267 n/m^3 and 65 n/m^3 in Feb., respectively and the simulated MPC in E, F, G and H are 74 n/m^3, 100 n/m^3, 145 n/m^3 and
268 72 n/m^3 in May, respectively. The simulated SMPC in adjacent sea area is shown in Fig.6 b. The average errors
269 between the measured and simulated values in Feb. and May are 10.6% and 13.4% in adjacent sea area, respectively
270 (Fig.6 b).
271 Compared with other regions, the errors in B, C, E and H are more significant. This may be due to the existence of
272 numerous non-point and point sources of MPs along the southeastern coast of China and Yangtze Estuary (Luo et al.
273 2019). Especially in May, since the Qiantang River is in the flood season and Taiwan's warm current is strong (Lian
274 et al. 2016), it may carry a huge number of MPs into adjacent sea area leading to simulated SMPC significantly lower
275 than measured SMPC. Ocean current is an important source of MPs (Genc et al. 2020).
276 Both the measured and simulated results indicate that compared with dry season (Feb.), the MPs are more likely to
277 disperse in flood season (May) leading to high SMPC in E and H. It is worth noting that the peak of SMPC in May

shift to the south (K point) in the research of Zhao et al. (Zhao et al. 2019). Two factors likely explain the southward shift of the peak of SMPC in May. First the strong Taiwan's warm current carries MPs into the southern adjacent sea area of Yangtze Estuary (Fig.6 a). Second the temporary surge in MPs abundance is formed due to wave, eddy current and other reasons resulting in deviation of field measurement results (Schmidt et al. 2018, van der Hal et al. 2017). The second hypothesis is based on the measured SMPC results of Liu et al. in June 2019, which showed that the peak of SMPC was still located in G (Liu, 2020).

Since the SMPC is obtained in dense grids and MPs form highly dispersed and polyphasic suspensions upon into waters, it is normal to detect some extreme values which are not found in field survey and some extreme values only occur in a few grids (Fig. 6b). Compared to previous studies only on the trajectory of MPs (Simantiris et al. 2022), the M-N method achieve the quantitative simulation with error less than 18%.

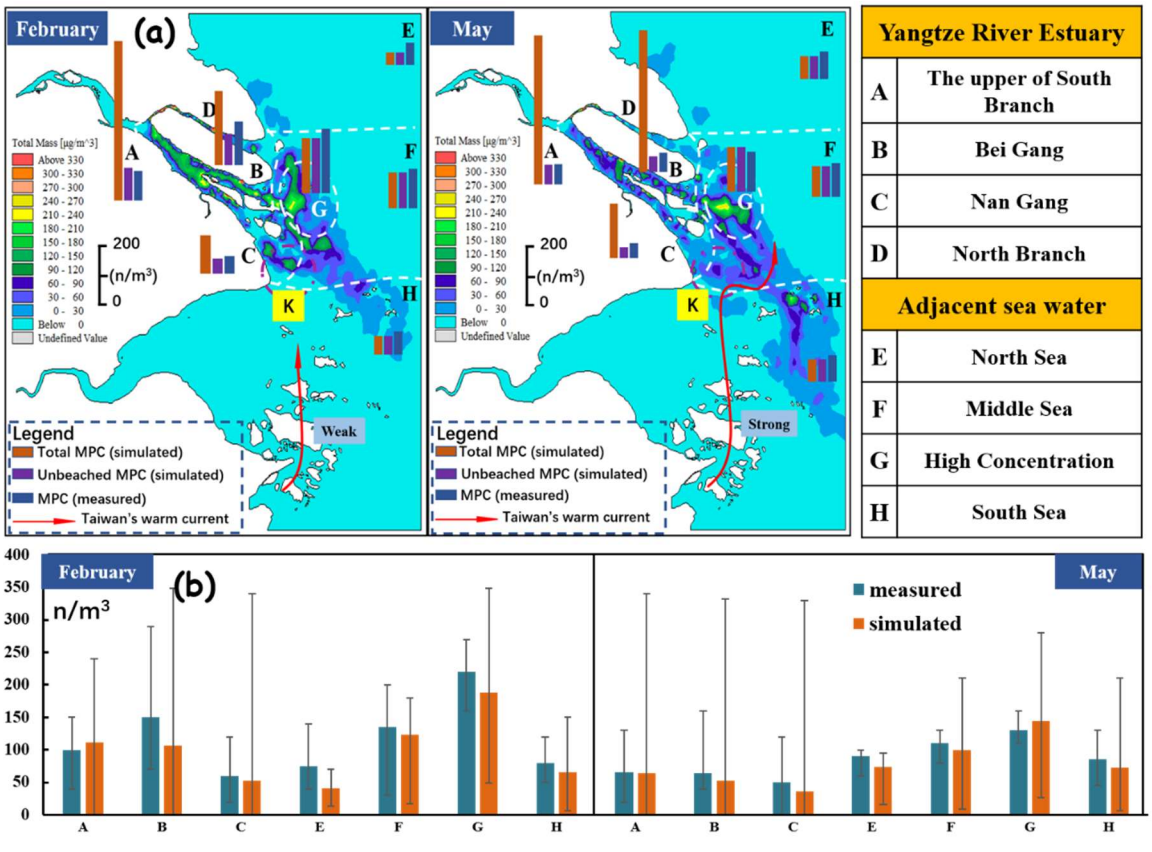

Figure 6 Model Performance, (a) Total microplastics concentration in simulation and spatial comparison of simulated and measured of suspended microplastics concentration; (b) Suspended microplastics concentration validation including max-min error bar.

3.2 Different Transport Patterns Simulation

Three types of MPs are simulated in biological sensitive period (Apr. 15 to May 15). PE and PVC are only beached, while PP is not only beached but also settled (Fig.7 a). The beaching ratio of PE, PP and PVC are 88.6%, 69.6% and 84.6%, respectively and the settlement ratio of PP is 9.8%. Thus, the sedimentation and sediment flocculation of MPs reduce the beaching of MPs. PP in suspension is observed to spread more slowly compared to PE and PVC, forming a smaller contamination area with smaller concentrations in the E and H regions. That maybe because vertical profile velocity is higher in the surface and lower in the bottom due to the bottom friction force. The result shows that the settlement can weaken the MPs transport effect of the tide, which means the horizontal diffusion of MPs is affected by the variation of vertical profile velocity (Yin et al. 2022). The TMPC ratios of PE MP, PP MP and PVC MP between B and C are 2.98, 2.5 and 1.45, respectively and the coefficient of variation of TMPC of PE MPs, PP MPs and PVC MPs among eight regions are 0.92, 0.79 and 0.73, respectively (Fig.7 b and Fig.8 b). These indicate that the concentration distribution of floating MPs varies greatly in space. The study in Delaware Bay also have indicated that the concentration of floating MPs varied greatly in space due to surface circulation (Cohen et al. 2019). Compared with PE MPs, PP MPs are less affected by surface circulation as the result of the continuous settlement. The concept of sediment inertia can well explain the relatively uniform concentration of PVC in space, that is, the huge inertia of suspended solid causes its transport to be relatively less susceptible to wind and current effects (Pizzuto et al. 2014). We also observe that the MPs flocculated with suspended solid have the widest diffusion range in Fig.7 a. Some studies have found that the suspended solid can enhance the MPs stability of MPs in water column (Andersen et al. 2021, Singh et al. 2019), which can also explain this phenomenon.

Overall, during biological sensitive period, the TMPC in Yangtze Estuary is around 4 times that of the adjacent sea area. In the Yangtze Estuary, salt wedge exists where salt and fresh water meet. This result may suggest that the salt wedge acts as a barrier for movement of MPs. The same phenomenon is also observed in Rio de la Plata (Acha et al.

2003). If only the suspended MPs are considered (Fig.8 b), the average SMPC in Yangtze Estuary is about 74n /m^3, which is lower than that in adjacent sea area (104n/m^3). This is consistent with the field survey results (Zhao et al. 2019). This indicates that lots of MPs are beached or settled in the estuary, especially on the north shore of the estuary and the North Branch (D). Although different transport patterns have little effect on the location of MPs aggregation areas, floating transported PE is more susceptible to current, resulting in higher beaching ratio and forming a more inhomogeneous concentration distribution compared with PVC transported with sediment flocculation and PP settled continuously. Additionally, the settlement can weaken the MPs transport effect of the tide. The risk of MPs in sensitive objectives in the estuary should be noticed.

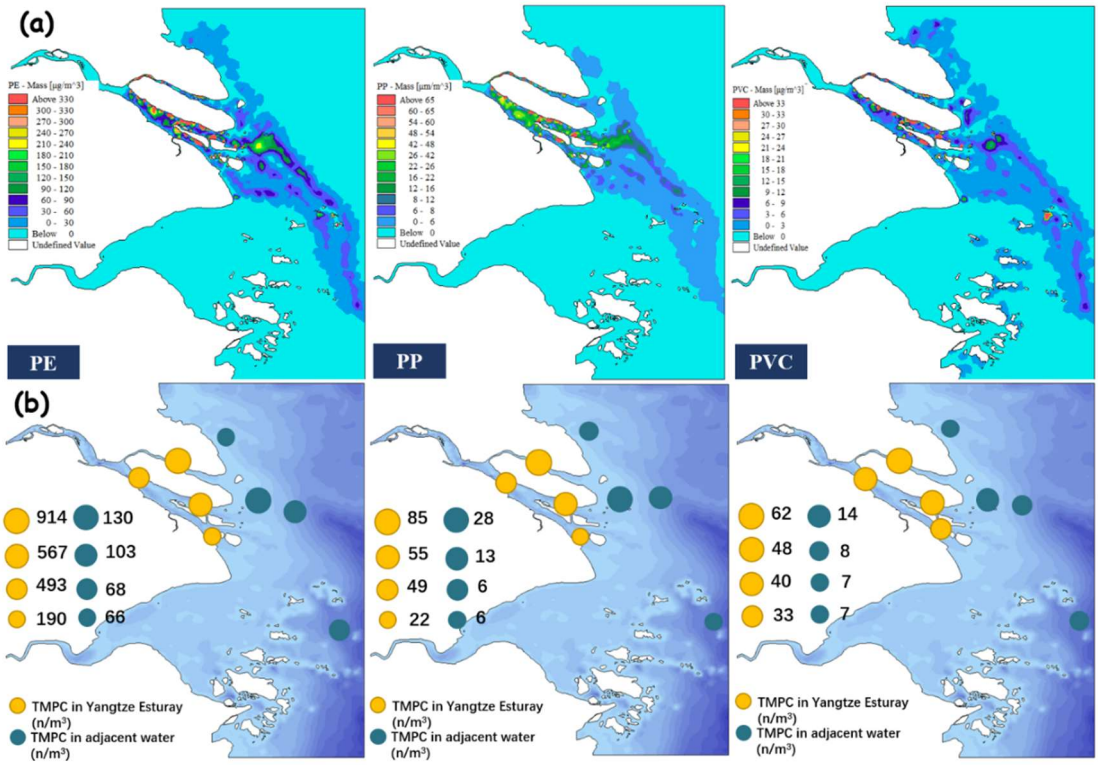

Figure 7 Total microplastics concentration in biological sensitive period, (a) The distribution of total microplastics concentration; (b) Total microplastics concentration in eight areas.

3.3 The distribution of MPs concentration

During all simulation periods it takes around 3-5 days for three types of MPs to enter the adjacent sea area. Then almost all the MPs from B rapidly gather in the southeast of Chongming Island (G) and form a “hot spot”. MPs stay

in G for a long time around 7 days. MPs begin to disperse to the seas in the northwest and southeast under the action of spring tides. A stable MPs pollution range is formed after around 15 days. In addition, the particle trajectory diagram shows that the MPs reciprocate in a straight line in the estuary and clockwise spiraled in the adjacent sea area (Fig.8 a). In the Yangtze Estuary, the inner part of the estuary is reciprocating flow while the water flow in the adjacent sea is clockwise under the observation by Li et al. (Li et al. 2017). Thus, the hydrodynamic conditions affect particle diffusion trajectories.

The distribution of TMPC in three periods is similar (Figure 7, Figure S1). When MPs enter the estuary, more MPs flow into B resulting in a significant higher TMPC in B than in C. That maybe because runoff in the Bei Gang (B) is greater than in the Nan Gang (C). The flow field is an essential factor in the distribution of MPs (Liu et al. 2021). Meanwhile, in the Yangtze Estuary, under the influence of geostrophic deflection, the north bank with low angle that is more likely to cause MPs beaching than south bank with steep angle (Fig. 5 a). This phenomenon also be observed in the São Vincente Estuary, Brazil (Cordeiro and Costa 2010). Additionally, the narrowing of north branch (D) also leads to more beaching of MPs. These phenomena imply that local topography influence the MPs behavior. In addition, the "hot spot" of MPs locates in the southeast of Chongming Island, overlapping the location of the Estuarine Turbidity Maximum and salt wedge (salinity front). This coincidence is also observed in the Guadalquivir estuary and the Delaware Bay (Bermudez et al. 2021, Cohen et al. 2019). This maybe because the energy dissipation of ebb and flow and the confluence of salt and fresh water occur at this position. It is worth noting that the runoff is too weak in the dry season, which leads to salt water flowing back into A through D, which may cause the TMPC of A is high in February. These results indicate that hydrodynamic conditions and topography are closely related to the distribution of TMPC. These rules have significance for judging the distribution of MPs concentration in other waters.

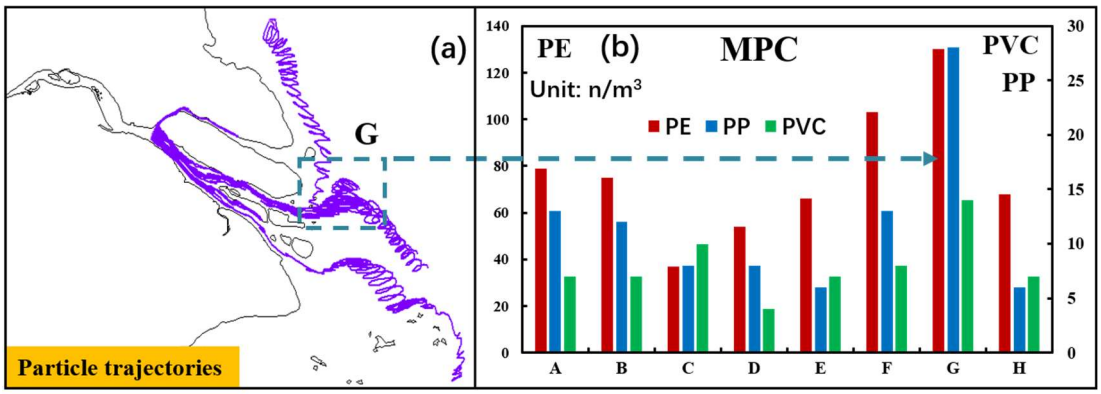

Figure 8 Particles trajectories and concentration, (a) Particles trajectories; (b) Suspended microplastics concentration in eight areas.

3.4 Risk Assessment

There are mainly three reservoirs and three animal refuges in the estuary (Fig.1). In the biological sensitive period, the MPs form some high concentration areas. Compared with the CH and QCS reservoirs, the DFXS reservoir on the north shore is more affected by MPs. In addition to concentration, the chemical composition affects the toxic effects of MPs (Zhang et al. 2022). In order to quantify the risk of MPs in sensitive objectives, HI and PLI are calculated according to formulas (1-4) in the Appendix (Fig.9). HI focuses on assessing risk from the chemical composition of MPs while PLI focuses on assessing risk from concentration. PVC MP is regarded as particle with much higher pollution risk than PE MP and PP MP. Based on HI value, we should focus on the conservation of species in SYECS and SCDNN, such as Chinese sturgeon and some migration birds. However, based on PLI value, we should focus on the risk of water use, especially in DFXS Reservoir, which is located on the north shore (Fig.1).

At present, there is no comprehensive and fixed standard for assessing the risk of MPs pollution. Common indicators are one-sided. Therefore, it is necessary to establish standards that can comprehensively reflect the risk of MPs pollution.

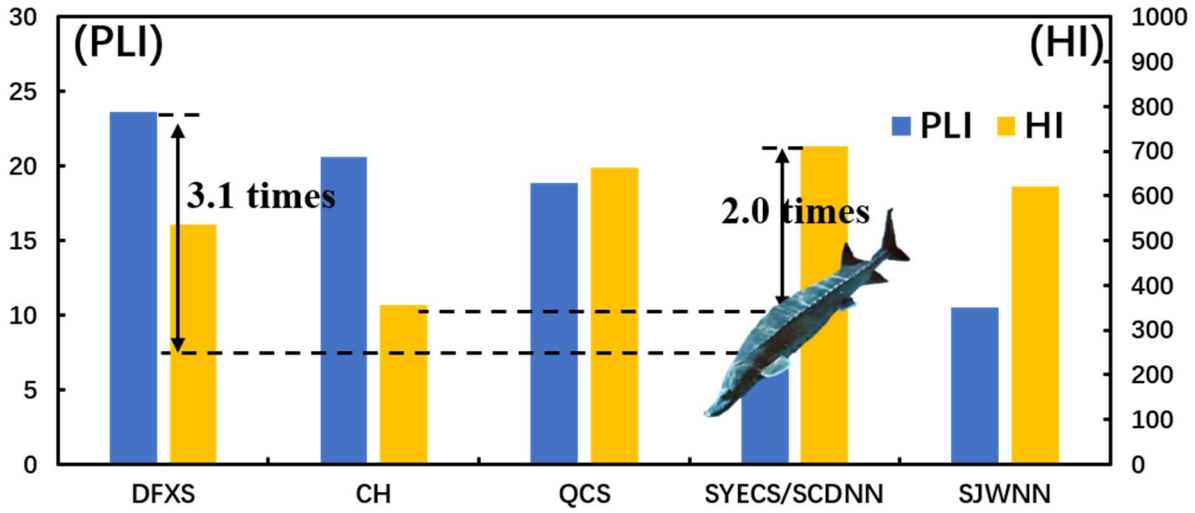

Figure 9 Microplastics risk assessment in sensitive targets

4 Conclusion

In this study, based on the previous sampling investigation, the first numerical simulation of MPs of the Yangtze Estuary which is considered as the largest plastic export is carried out. The quantitative simulation errors of different water seasons are both below 18%, which indicates the accuracy of simulation. The three types of MPs transport shows that floating transported PE is more susceptible to surface currents, beaching and forming more inhomogeneous concentration distribution compared with PVC transported with sediment flocculation and PP settled continuously. During all simulation periods, under the influence of surface current, local topography and salt wedge, high concentration of MPs is formed in the southeast of Chongming Island, north bank and the North Branch. About 57%~90% of MPs are settled or beached in the estuary, especially on the north shore. Thus, the MPs risk is noticed during the biological sensitive period. HI focusing on the chemical composition of MPs indicates that the conservation of species in SYECS and SCDNN should be considered while PLI focusing on MPC indicates that the water safety of the DFXS Reservoir should be considered.

Our results explore the fate of MPs in the Yangtze Estuary. However, pollution sources within and near the Yangtze Estuary and the ocean current also affect the MPC. Meanwhile, the resuspension, aging, biofouling and solid-liquid distribution of MPs should be further studied to improve the simulation accuracy.

Declaration of competing interest

None

Acknowledgements

This work was supported by the Major Science and Technology Program for Water Pollution Control and Treatment of China (2017ZX07203002-01), Shanghai Water Bureau Research project (Assessment of the Impact of Salinity Fluctuation in the Yangtze Estuary on Water Quality of Drinking Water Sources, 2019-09), Water conservancy science and technology project of Jiangxi Province (KT201623), National Natural Science Foundation of China (No.51779075), A Project Funded by the Priority Academic Program Development of Jiangsu Higher Education Institutions (No. 51479064).

Reference

Acha, E.M., Mianzan, H.W., Iribarne, O., Gagliardini, D.A., Lasta, C. and Daleo, P. (2003) The role of the Rio de la Plata bottom salinity front in accumulating debris. Marine Pollution Bulletin 46(2), 197-202.

Alosairi, Y., Al-Salem, S.M. and Al Ragum, A. (2020) Three-dimensional numerical modelling of transport, fate and distribution of microplastics in the northwestern Arabian/Persian Gulf. Marine Pollution Bulletin 161, 15.

Andersen, T.J., Rominikan, S., Olsen, I.S., Skinnebach, K.H. and Fruergaard, M. (2021) Flocculation of PVC Microplastic and Fine-Grained Cohesive Sediment at Environmentally Realistic Concentrations. Biological Bulletin 240(1), 42-51.

Atwood, E.C., Falcieri, F.M., Piehl, S., Bochow, M., Matthies, M., Franke, J., Carniel, S., Sclavo, M., Laforsch, C. and Siegert, F. (2019) Coastal accumulation of microplastic particles emitted from the Po River, Northern Italy: Comparing remote sensing and hydrodynamic modelling with in situ sample collections. Marine Pollution Bulletin 138, 561-574.

Besseling, E., Quik, J.T.K., Sun, M. and Koelmans, A.A. (2017) Fate of nano- and microplastic in freshwater systems:

403 A modeling study. Environmental Pollution 220, 540-548.
404 Bermudez, M., Vilas, C., Quintana, R., Gonzalez-Fernandez, D., Cozar, A. and Diez-Minguito, M. (2021) Unravelling
405 spatio-temporal patterns of suspended microplastic concentration in the Natura 2000 Guadalquivir estuary (SW
406 Spain): Observations and model simulations. Marine Pollution Bulletin 170, 11.
407 Carpente.Ej, Anderson, S.J., Miklas, H.P., Peck, B.B. and Harvey, G.R. (1972) POLYSTYRENE SPHERULES IN
408 COASTAL WATERS. Science 178(4062), 749-&.
409 Castelvetro, V., Corti, A., Bianchi, S., Ceccarini, A., Manariti, A. and Vinciguerra, V. (2020) Quantification of
410 poly(ethylene terephthalate) micro- and nanoparticle contaminants in marine sediments and other environmental
411 matrices. Journal of Hazardous Materials 385, 8.
412 Chubarenko, I., Bagaev, A., Zobkov, M. and Esiukova, E. (2016) On some physical and dynamical properties of
413 microplastic particles in marine environment. Marine Pollution Bulletin 108(1-2), 105-112.
414 Cohen, J.H., Internicola, A.M., Mason, R.A. and Kukulka, T. (2019) Observations and Simulations of Microplastic
415 Debris in a Tide, Wind, and Freshwater-Driven Estuarine Environment: the Delaware Bay. Environmental Science &
416 Technology 53(24), 14204-14211.
417 Collins, C. and Hermes, J.C. (2019) Modelling the accumulation and transport of floating marine micro-plastics
418 around South Africa. Marine Pollution Bulletin 139, 46-58.
419 Cordeiro, C. and Costa, T.M. (2010) Evaluation of solid residues removed from a mangrove swamp in the Sao Vicente
420 Estuary, SP, Brazil. Marine Pollution Bulletin 60(10), 1762-1767.
421 Derraik, J.G.B. (2002) The pollution of the marine environment by plastic debris: a review. Marine Pollution Bulletin
422 44(9), 842-852.
423 DHI, 2011a. MIKE 21 Flow Model FM: Hydrodynamic Module, User Guide. Danish Hydraulic Institute Water and
424 Environment, Hørsholm, Denmark.

DHI, 2011c. MIKE 21 Flow Model FM: Mud Transport Module, User Guide. Danish Hydraulic Institute Water and Environment, Hørsholm, Denmark.

DHI, 2011d. MIKE 21 Flow Model FM: Particle Tracking Module, User Guide. Danish Hydraulic Institute Water and Environment, Hørsholm, Denmark.

Ding, Y., Liu, H.F. and Yang, W. (2019) Numerical Prediction of the Short-Term Trajectory of Microplastic Particles in Laizhou Bay. Water 11(11), 17.

Dioguardi, F., Mele, D. and Dellino, P. (2018) A New One-Equation Model of Fluid Drag for Irregularly Shaped Particles Valid Over a Wide Range of Reynolds Number. Journal of Geophysical Research-Solid Earth 123(1), 144-156.

Dubaish, F. and Liebezeit, G. (2013) Suspended Microplastics and Black Carbon Particles in the Jade System, Southern North Sea. Water Air and Soil Pollution 224(2), 8.

Farrell, P. and Nelson, K. (2013) Trophic level transfer of microplastic: Mytilus edulis (L.) to Carcinus maenas (L.). Environmental Pollution 177, 1-3.

Feng, L., Hu, C.M., Chen, X.L. and Song, Q.J. (2014) Influence of the Three Gorges Dam on total suspended matters in the Yangtze Estuary and its adjacent coastal waters: Observations from MODIS. Remote Sensing of Environment 140, 779-788.

Fisher, N.S., Bjerregaard, P. and Fowler, S.W. (1983) INTERACTIONS OF MARINE PLANKTON WITH TRANSURANIC ELEMENTS .1. BIOKINETICS OF NEPTUNIUM, PLUTONIUM, AMERICIUM, AND CALIFORNIUM IN PHYTOPLANKTON. Limnology and Oceanography 28(3), 432-447.

Gao, Y., Gao, L., Zhu, L. and Li, D. (2018) Spatiotemporal variations in concentration and size of suspended particulate matter in the Changjiang(Yangtze River)Estuary and its adjacent sea. Acta Oceanologica Sinica 40(3), 62-73.

Genc, A.N., Vural, N. and Balas, L. (2020) Modeling transport of microplastics in enclosed coastal waters: A case study in the Fethiye Inner Bay. Marine Pollution Bulletin 150, 17.

He, D., Chen, X.J., Zhao, W., Zhu, Z.Q., Qi, X.J., Zhou, L.F., Chen, W., Wan, C.Y., Li, D.W., Zou, X. and Wu, N. (2021) Microplastics contamination in the surface water of the Yangtze River from upstream to estuary based on different sampling methods. Environmental Research 196, 9.

Huffer, T., PraetoriusP'll, A., Wagner, S., von der Kammer, F. and Hofiliannte, T. (2017) Microplastic Exposure Assessment in Aquatic Environments: Learning from Similarities and Differences to Engineered Nanoparticles. Environmental Science & Technology 51(5), 2499-2507.

Iwasaki, S., Isobe, A., Kako, S., Uchida, K. and Tokai, T. (2017) Fate of microplastics and mesoplastics carried by surface currents and wind waves: A numerical model approach in the Sea of Japan. Marine Pollution Bulletin 121(1-2), 85-96.

Jalon-Rojas, I., Wang, X.H. and Fredj, E. (2019) A 3D numerical model to Track Marine Plastic Debris (TrackMPD): Sensitivity of microplastic trajectories and fates to particle dynamical properties and physical processes. Marine Pollution Bulletin 141, 256-272.

Kaiser, D., Kowalski, N. and Waniek, J.J. (2017) Effects of biofouling on the sinking behavior of microplastics. Environmental Research Letters 12(12), 10. Kaiser, D., Kowalski, N. and Waniek, J.J. (2017) Effects of biofouling on the sinking behavior of microplastics. Environmental Research Letters 12(12), 10.

Khatmullina, L. and Isachenko, I. (2017) Settling velocity of microplastic particles of regular shapes. Marine Pollution Bulletin 114(2), 871-880.

Kooi, M., van Nes, E.H., Scheffer, M. and Koelmans, A.A. (2017) Ups and Downs in the Ocean: Effects of Biofouling on Vertical Transport of Microplastics. Environmental Science & Technology 51(14), 7963-7971.

Kowalski, N., Reichardt, A.M. and Waniek, J.J. (2016) Sinking rates of microplastics and potential implications of

their alteration by physical, biological, and chemical factors. Marine Pollution Bulletin 109(1), 310-319.

Lagarde, F., Olivier, O., Zanella, M., Daniel, P., Hiard, S. and Caruso, A. (2016) Microplastic interactions with freshwater microalgae: Hetero-aggregation and changes in plastic density appear strongly dependent on polymer type. Environmental Pollution 215, 331-339.

Lian, E.G., Yang, S.Y., Wu, H., Yang, C.F., Li, C. and Liu, J.T. (2016) Kuroshio subsurface water feeds the wintertime Taiwan Warm Current on the inner East China Sea shelf. Journal of Geophysical Research-Oceans 121(7), 4790-4803.

Li, C.C., Gan, Y.D., Zhang, C., He, H., Fang, J.H., Wang, L.F., Wang, Y. and Liu, J. (2021) "Microplastic communities" in different environments: Differences, links, and role of diversity index in source analysis. Water Research 188, 11.

Li, L., Geng, S.X., Wu, C.X., Song, K., Sun, F.H., Visvanathan, C., Xie, F.Z. and Wang, Q.L. (2019) Microplastics contamination in different trophic state lakes along the middle and lower reaches of Yangtze River Basin. Environmental Pollution 254, 9.

Ling, S.D., Sinclair, M., Levi, C.J., Reeves, S.E. and Edgar, G.J. (2017) Ubiquity of microplastics in coastal seafloor sediments. Marine Pollution Bulletin 121(1-2), 104-110.

Li, P., Shi, B.W., Wang, Y.P., Qin, W.H., Li, Y.G. and Chen, J. (2017) Analysis of the characteristics of offshore currents in the Changjiang (Yangtze River) estuarine waters based on buoy observations. Acta Oceanologica Sinica 36(4), 13-20.

Liu Y.(2020) The role of rivers and coastal lakes in the transport of plastic particles from terrestrial sources to the Marine environment[D]. Shanghai Ocean University. (Chinese)

Liu, K., Zhang, Z.W., Wu, H., Wang, J.X., Wang, R., Zhang, T., Feng, Z.H. and Li, D.J. (2021) Accumulation of microplastics in a downstream area of a semi-enclosed bay: Implications of input from coastal currents. Science of

491 the Total Environment 791, 9.

492 Li, Y.B., Lu, Z.B., Zheng, H.Y., Wang, J. and Chen, C. (2020) Microplastics in surface water and sediments of

493 Chongming Island in the Yangtze Estuary, China. Environmental Sciences Europe 32(1), 12.

494 Li, Y., Wang, X.J., Fu, W.Y., Xia, X.H., Liu, C.Q., Min, J.C., Zhang, W. and Crittenden, J.C. (2019) Interactions

495 between nano/micro plastics and suspended sediment in water: Implications on aggregation and settling. Water

496 Research 161, 486-495.

497 Long, M., Moriceau, B., Gallinari, M., Lambert, C., Huvet, A., Raffray, J. and Soudant, P. (2015) Interactions between

498 microplastics and phytoplankton aggregates: Impact on their respective fates. Marine Chemistry 175, 39-46.

499 Long, M., Paul-Pont, I., Hegaret, H., Moriceau, B., Lambert, C., Huvet, A. and Soudant, P. (2017) Interactions

500 between polystyrene microplastics and marine phytoplankton lead to species-specific hetero-aggregation.

501 Environmental Pollution 228, 454-463.

502 Luo, W.Y., Su, L., Craig, N.J., Du, F.N., Wu, C.X. and Shi, H.H. (2019) Comparison of microplastic pollution in

503 different water bodies from urban creeks to coastal waters. Environmental Pollution 246, 174-182.

504 Macleod, A.K., Stanley, M.S., Day, J.G. and Cook, E.J. (2016) Biofouling community composition across a range of

505 environmental conditions and geographical locations suitable for floating marine renewable energy generation.

506 Biofouling 32(3), 261-276.

507 Mai, L., Sun, X.F., Xia, L.L., Bao, L.J., Liu, L.Y. and Zeng, E.Y. (2020) Global Riverine Plastic Outflows.

508 Environmental Science & Technology 54(16), 10049-10056.

509 Pizzuto, J., Schenk, E.R., Hupp, C.R., Gellis, A., Noe, G., Williamson, E., Karwan, D.L., O'Neal, M., Marquard, J.,

510 Aalto, R. and Newbold, D. (2014) Characteristic length scales and time-averaged transport velocities of suspended

511 sediment in the mid-Atlantic Region, USA. Water Resources Research 50(2), 790-805.

512 Pohl, F., Eggenhuisen, J.T., Kane, I.A. and Clare, M.A. (2020) Transport and Burial of Microplastics in Deep-Marine

513 Sediments by Turbidity Currents. Environmental Science & Technology 54(7), 4180-4189.

514 Schmidt, C., Krauth, T. and Wagner, S. (2018) Export of Plastic Debris by Rivers into the Sea (vol 51, pg 12246,

515 2017). Environmental Science & Technology 52(2), 927-927.

516 Schmidt, N., Thibault, D., Galgani, F., Paluselli, A. and Sempere, R. (2018) Occurrence of microplastics in surface

517 waters of the Gulf of Lion (NW Mediterranean Sea). Progress in Oceanography 163, 214-220.

518 Simantiris, N., Avlonitis, M. and Theocharis, A. (2022) Simulation of the transport of marine microplastic particles

519 in the Ionian Archipelago (NE Ionian Sea) using a Lagrangian model and the control mechanisms affecting their

520 transport. Journal of hazardous materials 437, 129349.

521 Singh, N., Tiwari, E., Khandelwal, N. and Darbha, G.K. (2019) Understanding the stability of nanoplastics in aqueous

522 environments: effect of ionic strength, temperature, dissolved organic matter, clay, and heavy metals. Environmental

523 Science-Nano 6(10), 2968-2976.

524 Shen, M.C., Zeng, Z.T., Song, B., Yi, H., Hu, T., Zhang, Y.X., Zeng, G.N. and Xiao, R. (2021) Neglected microplastics

525 pollution in global COVID-19: Disposable surgical masks. Science of the Total Environment 790, 10.

526 van der Hal, N., Ariel, A. and Angel, D.L. (2017) Exceptionally high abundances of microplastics in the oligotrophic

527 Israeli Mediterranean coastal waters. Marine Pollution Bulletin 116(1-2), 151-155.

528 Waldschlager, K. and Schuttrumpf, H. (2019) Effects of Particle Properties on the Settling and Rise Velocities of

529 Microplastics in Freshwater under Laboratory Conditions. Environmental Science & Technology 53(4), 1958-1966.

530 Wang, H., Yan, H.Y., Zhou, F.N., Li, B., Zhuang, W. and Shen, Y.H. (2020) Changes in nutrient transport from the

531 Yangtze River to the East China Sea linked to the Three-Gorges Dam and water transfer project. Environmental

532 Pollution 256, 11.

533 Yin, M.C., Cao, H.J., Zhao, W.L., Wang, T., Huang, W. and Cai, M.G. (2022) Tide-driven microplastics transport in

534 an elongated semi-closed bay: A case study in Xiangshan Bay, China. Science of the Total Environment 846, 11.

Yin, K., Wang, D.X., Zhao, H.J., Wang, Y., Guo, M.H., Liu, Y.C., Li, B.Y. and Xing, M.W. (2021) Microplastics pollution and risk assessment in water bodies of two nature reserves in Jilin Province: Correlation analysis with the degree of human activity. Science of the Total Environment 799, 14.

Wang, M.H., He, Y.D. and Sen, B. (2019) Research and management of plastic pollution in coastal environments of China. Environmental Pollution 248, 898-905.

Wang, X.J., Bolan, N., Tsang, D.C.W., Sarkar, B., Bradney, L. and Li, Y. (2021) A review of microplastics aggregation in aquatic environment: Influence factors, analytical methods, and environmental implications. Journal of Hazardous Materials 402, 19.

Welden, N.A. and Cowie, P.R. (2017) Degradation of common polymer ropes in a sublittoral marine environment. Marine Pollution Bulletin 118(1-2), 248-253.

Williams, A.T. and Simmons, S.L. (1999) Sources of riverine litter: The River Taff, South Wales, UK. Water Air and Soil Pollution 112(1-2), 197-216.

Xiong, X., Wu, C.X., Elser, J.J., Mei, Z.G. and Hao, Y.J. (2019) Occurrence and fate of microplastic debris in middle and lower reaches of the Yangtze River - From inland to the sea. Science of the Total Environment 659, 66-73.

Xu, P., Peng, G.Y., Su, L., Gao, Y.Q., Gao, L. and Li, D.J. (2018) Microplastic risk assessment in surface waters: A case study in the Changjiang Estuary, China. Marine Pollution Bulletin 133, 647-654.

Yuan, W.K., Christie-Oleza, J.A., Xu, E.G., Li, J.W., Zhang, H.B., Wang, W.F., Lin, L., Zhang, W.H. and Yang, Y.Y. (2022) Environmental fate of microplastics in the world's third-largest river: Basin-wide investigation and microplastic community analysis. Water Research 210, 10.

Zeng, Y.C., Wang, H., Liang, D.F., Yuan, W.H., Li, B., Zhuang, W., Kaisam, J.P. and Shen, W.B. (2021) Quantifying wind-induced impacts on particulate Cu footprint in the Yangtze Estuary. Chemosphere 264, 12.

Zhang, C.F., Wang, C.Y., Cao, G.L., Wang, D.W. and Ho, S.H. (2020) A sustainable solution to plastics pollution: An

557 eco-friendly bioplastic film production from high-salt contained Spirulina sp. residues. Journal of Hazardous
558 Materials 388, 10.
559 Zhang, F., Peng, G.Y., Xu, P., Zhu, L.X., Li, C.J., Wei, N. and Li, D.J. (2022) Ecological risk assessment of marine
560 microplastics using the analytic hierarchy process: A case study in the Yangtze River Estuary and adjacent marine
561 areas. Journal of Hazardous Materials 425, 8.
562 Zhang, H. (2017) Transport of microplastics in coastal seas. Estuarine Coastal and Shelf Science 199, 74-86.
563 Zhang, J.Q. and Choi, C.E. (2022) Improved Settling Velocity for Microplastic Fibers: A New Shape-Dependent Drag
564 Model. Environmental Science & Technology 56(2), 962-973.
565 Zhang, Z.Y., Mamat, Z. and Chen, Y.G. (2020) Current research and perspective of microplastics (MPs) in soils (dusts)
566 rivers (lakes), and marine environments in China. Ecotoxicology and Environmental Safety 202, 9.
567 Zhao, S.Y., Wang, T., Zhu, L.X., Xu, P., Wang, X.H., Gao, L. and Li, D.J. (2019) Analysis of suspended microplastics
568 in the Changjiang Estuary: Implications for riverine plastic load to the ocean. Water Research 161, 560-569.
569 Zhao, S.Y., Zhu, L.X., Wang, T. and Li, D.J. (2014) Suspended microplastics in the surface water of the Yangtze
570 Estuary System, China: First observations on occurrence, distribution. Marine Pollution Bulletin 86(1-2), 562-568.
571 Zhu, X. and Zeng, Y.H. (2016) Settling velocity of non-spherical hydrochorous seeds, pp. 990-996, China Ocean
572 Press, Wuxi, PEOPLES R CHINA.